



Article

# Simultaneous Electrochemical Sensing of Dopamine, Ascorbic Acid, and Uric Acid Using Nitrogen-Doped Graphene Sheet-Modified Glassy Carbon Electrode

Hediyeh Moradpour<sup>1</sup> and Hadi Beitollahi<sup>2,\*</sup> 

<sup>1</sup> Department of Chemistry, Graduate University of Advanced Technology, Kerman P.O. Box 876318-85356, Iran

<sup>2</sup> Environment Department, Institute of Science and High Technology and Environmental Sciences, Graduate University of Advanced Technology, Kerman P.O. Box 876318-85356, Iran

\* Correspondence: h.beitollahi@yahoo.com; Tel.: +98-3426226613; Fax: +98-3426226613

**Abstract:** Nitrogen (N) doping is a well-known approach that can be effectively used to tune the properties of graphene-supported materials. The current attempt followed a simple hydrothermal protocol for the fabrication of N-doped graphene sheets (N-GSs). The N-GSs were subsequently applied to modify the surface of a glassy carbon electrode (GCE) for a dopamine (DA) electrochemical sensor (N-GSs/GCE), tested on the basis of differential pulse voltammetry (DPV). The findings highlighted a limit of detection (LOD) as narrow as 30 nM and a linear response in the concentration range between 0.1 and 700.0  $\mu$ M. The modified electrode could successfully determine DA in the co-existence of uric acid (UA) and ascorbic acid (AA), the results of which verified the potent electrocatalytic performance of the proposed sensor towards AA, DA, and UA oxidation, and three distinct voltammetric peaks at 110, 250, and 395 mV via DPV. The practical applicability of the as-developed N-GSs/GCE sensor was confirmed by sensing the study analytes in real specimens, with satisfactory recovery rates.

**Keywords:** nitrogen-doped graphene sheets; glassy carbon electrode; dopamine; uric acid; ascorbic acid



**Citation:** Moradpour, H.; Beitollahi, H. Simultaneous Electrochemical Sensing of Dopamine, Ascorbic Acid, and Uric Acid Using Nitrogen-Doped Graphene Sheet-Modified Glassy Carbon Electrode. *C* **2022**, *8*, 50.  
<https://doi.org/10.3390/c8040050>

Academic Editor: Giuseppe Cirillo

Received: 30 August 2022

Accepted: 14 September 2022

Published: 3 October 2022

**Publisher's Note:** MDPI stays neutral with regard to jurisdictional claims in published maps and institutional affiliations.



**Copyright:** © 2022 by the authors. Licensee MDPI, Basel, Switzerland. This article is an open access article distributed under the terms and conditions of the Creative Commons Attribution (CC BY) license (<https://creativecommons.org/licenses/by/4.0/>).

## 1. Introduction

3,4-dihydroxyphenethylamine, or dopamine (DA), as a key neurotransmitter, is positioned in the family of excitatory chemical neurotransmitters. It is capable of regulating human cognition and emotions, and exists as a main catecholamine in the central nervous system (CNS). The mean DA content in blood and serum samples of human beings can range from  $10^{-6}$  to  $10^{-9}$  mol/L [1,2]. DA has an extensive presence in mammalian brain tissues and body fluids. It is significantly involved in some processes performed in the CNS, metabolic system, kidneys, cardiovascular system, and hormonal actions. Hence, any change in the level of DA in different parts of the body can be indicative of diverse neurological problems such as Parkinson's disease, Alzheimer's disease, Huntington's disease, and addiction. DA can be a biochemical precursor for catechol amine neurotransmitters, epinephrine, and norepinephrine [3–5]. Accordingly, there is a need for a sensitive, simple, and selective approach to determine and quantify the DA for early diagnosis of relevant medical conditions.

There are some analytical methods for determination of DA, some of which include chemiluminescence [6], chromatography [7], colorimetry [8], fluorescence [9], and capillary electrophoresis [10]. In spite of the valuable advantages of these techniques, they suffer from some shortcomings such as long testing time, high cost, and tedious pretreatment processes. Hence, considerable attention has been recently focused on electrochemical approaches in determination of electroactive analytes because of their commendable merits such as high sensitivity, low cost, and fast reaction [11–21]. Nevertheless, the presence of some interferants such as uric acid (UA) and ascorbic acid (AA) can disrupt the detection

of DA [22,23]. This problem can be particularly aggravated with the use of bare electrodes due to some deficiencies such as overlapping oxidation potentials and marked electrode fouling, commonly leading to poor selectivity and reproducibility. This bottleneck can be circumvented by modifying the electrode surface using different modifiers [24,25]. In general, chemically modified electrodes lead to an increase in sensitivity and selectivity for the determination of various analytes [26–33].

The unique chemical and physical properties of nanomaterials make them extremely convenient for applications in various fields [34–40]. Nanomaterials are among the best candidates to create ultra-sensitive and ultra-selective electrochemical sensors due to their appreciable electro-conductivity and huge surface area [41–49].

Graphene with a 2D layer of C atoms in a honeycomb configuration have shown unparalleled electrical, mechanical, chemical, and optical properties. They can act as potent electrode modifiers due to huge surface area, high electro-conductivity, great chemical and thermal stability, and mechanical strength [50–52]. Reportedly, chemical doping of graphene can trigger semiconducting properties; thus, N-doped or P-doped graphene can experience high charge conductivity and chemical reactivity [53]. N-doping can be highly effective in the regulation of electronic activity and mechanical properties and in the elevation of the electrocatalytic performance of carbon materials [54]. N-doped graphene sheets (N-GSs) have been promising options in the fabrication of electrochemical (bio)sensors, supercapacitors, batteries, and electrocatalysis, because they possess huge surface area, great electric conductivity, subtle electronic traits, a large number of edge sites to adsorb electroactive molecules, catalytic capacity, and appreciable electron density [55–57].

The current attempt followed a simple hydrothermal protocol for the fabrication of N-GSs. The N-GSs was subsequently applied to modify the surface of a GCE to create a DA electrochemical sensor (NGSs/GCE), even in the co-existence of UA and AA, tested on the basis of DPV. The practical applicability of the as-developed NGSs/GCE sensor was examined by sensing the study analytes in real specimens.

## 2. Experimental

### 2.1. Instruments and Chemicals

An Autolab PGSTAT 320N Potentiostat/Galvanostat Analyzer ((Eco-Chemie, Utrecht, The Netherlands)) with GPES (General Purpose Electrochemical System-version 4.9) software was applied for all electrochemical determinations at ambient temperature. A Metrohm 713 pH-meter with glass electrodes (Metrohm AG, Herisau, Switzerland) was used to determine and adjust the solution pH.

All solvents and chemicals applied in our protocol were of analytical grade from Merck and Sigma-Aldrich. Phosphate buffer solution (PBS) was prepared by phosphoric acid and adjusted by NaOH to the desired pH value.

### 2.2. Synthesis of N-GSs

The synthesis of N-GSs was based on the hydrothermal protocol using the base material graphene oxide (GO) and the reducing and doping agent urea. Thus, 100.0 mg of exfoliated GO was dissolved in 100 mL of deionized water under ultra-sonication, with the solution pH adjusted to 10.0 using  $\text{NH}_3 \cdot \text{H}_2\text{O}$  (30%), followed by adding 6.0 g of urea under 3 h ultra-sonication. Next, the resultant mixture was placed in a Teflon-lined autoclave at 180 °C for 12 h, followed by cooling to room temperature. After collecting N-GSs, washing was done thoroughly with water and the pH was adjusted to a neutral value. Eventually, the freeze-drying process was done.

### 2.3. Preparation of the N-GSs/GCE Sensor

A drop-casting technique was followed to fabricate the N-GSs/GCE. Thus, a certain amount of as-prepared N-GSs (1.0 mg) was subsequently dispersed in deionized water (1.0 mL) under 25-min ultra-sonication. Then, the prepared suspension (4.0  $\mu\text{L}$ ) was coated on the GCE surface dropwise and dried at the laboratory temperature.

The surface areas of the N-GSs/GCE and the bare GCE were obtained by CV using 1.0 mM  $K_3Fe(CN)_6$  at different scan rates. Using the Randles–Sevcik equation [58] for N-GSs/GCE, the electrode surface was found to be 0.119 cm<sup>2</sup>, about 3.8 times greater than bare GCE.

### 3. Results and discussion

#### 3.1. Characterization of N-GSs

Figure 1 shows the characterization of GO and N-GSs using XRD. According to the XRD pattern for GO (Figure 1a), a peak can be seen at the  $2\theta$  value of  $11.5^\circ$  (inter-planer space = 7.69 Å). A larger inter-planer space can be observed for GO in comparison to graphite, which can be attributed to the presence of H<sub>2</sub>O molecules and diverse oxygen groups on its surface. The XRD pattern captured for the N-GSs highlighted a high degree of reduction (Figure 1b). Following the hydrothermal reactions and together with the N-doping process, the disappearance of the peak at  $2\theta = 11.5^\circ$  confirmed the successful GO reduction, but the N-GSs pattern created a wide peak at  $24.7^\circ$  [59], related to the inter-planar distance of 3.602 Å, which provides  $\pi$ – $\pi$  stacking between graphene sheets [60].

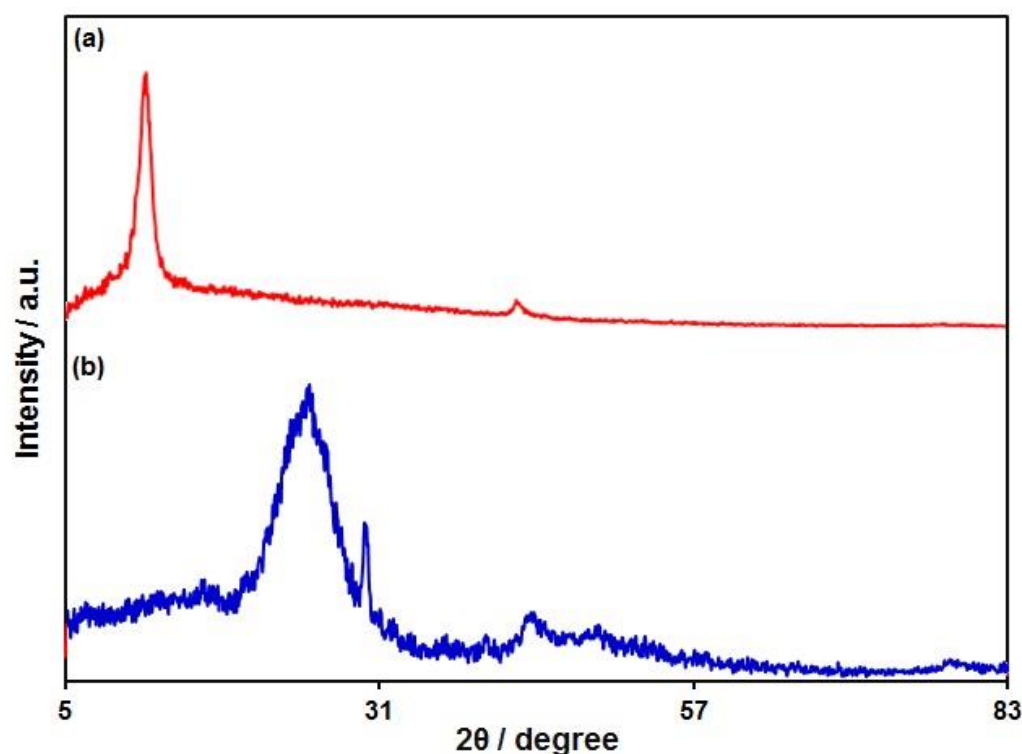


Figure 1. XRD pattern of (a) GO and (b) N-GSs.

Figure 2 compares the FT-IR spectra captured from GO and N-GSs. In the FT-IR spectrum of GO, there are different functional groups that are shown in Figure 2a. On account of these characteristic peaks, multiple oxygen (O)-containing functional groups, such as epoxy, hydroxyl, and carboxyl, were present on the GO surface. The lack of absorption peaks of oxygen groups in the N-GSs showed the effective reduction of GO during the hydrothermal process. Two peaks appeared at 1184 and 1562 cm<sup>-1</sup> related to C–N and C=N (occasionally, C=C and C=N bonds are stretched at the identical wavelength), respectively. Therefore, the graphene was N-doped successfully.

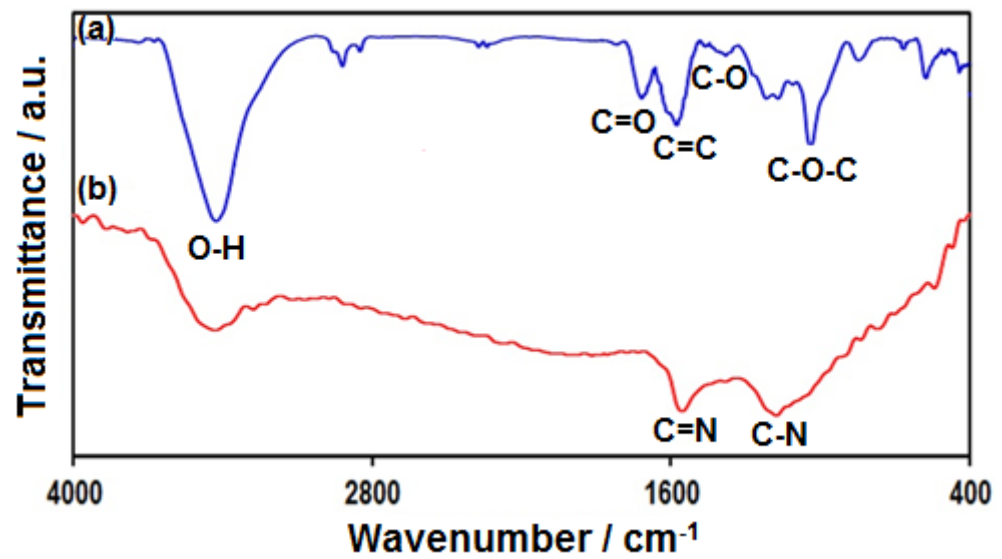


Figure 2. FT-IR spectra of (a) GO and (b) N-GSs.

As shown in Figure 3 depicting the FE-SEM image captured for the N-GSs, the N-GSs maintained the ultrathin flexible 2D structure of pristine graphene; and the N-GS sheets possessed a wave structure similar to thin wrinkled paper, representing the successful N-doping process for the graphene.

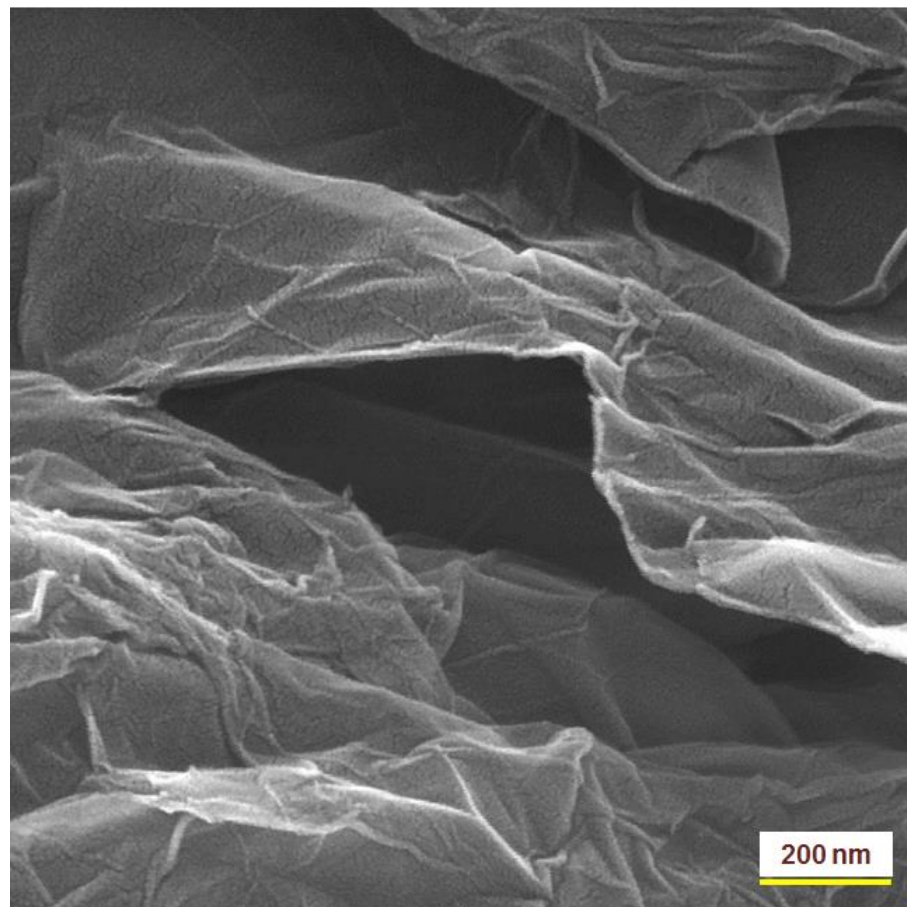
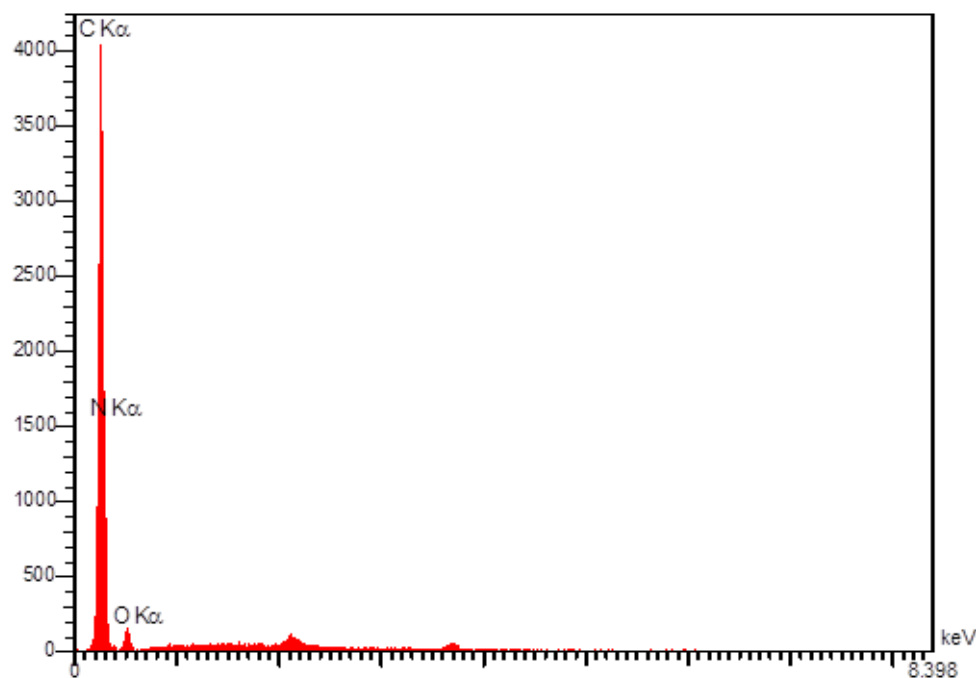


Figure 3. The FE-SEM image of the NGSs.

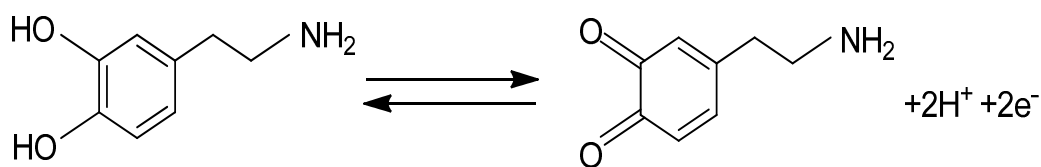
Figure 4 shows the energy dispersive X-ray spectroscopy (EDS) analysis in determining the chemical composition of the N-GSs, the findings of which showed C (80.4%), N (16.3%), and O (3.3%) present in the prepared sample.



**Figure 4.** EDS spectrum of N-GSs.

### 3.2. Electrochemical Response of DA at the Various Electrodes Surfaces

The electrochemical response of DA in the 0.1 M PBS adjusted to variable pH values (2.0 to 9.0) was explored to determine the influence of the electrolyte solution pH. The results showed that the redox peaks of DA depended on the pH value, with these reaching a maximum with increasing pH up to 7.0 and then decreasing with greater pH values. Hence, the pH value of 7.0 was considered to be the optimum for subsequent electrochemical determinations. The reaction mechanism of DA is shown in Scheme 1.



**Scheme 1.** Electrochemical oxidation mechanism of DA at the surface of NGSs/GCE.

The cyclic voltammograms (CVs) were captured for the DA (200.0  $\mu$ M) on the bare GCE and NGSs/GCE to explore the electrocatalytic performance of the N-GSs (Figure 5). Figure 5 illustrates two weak oxidation and reduction peaks on the bare GCE with oxidation peak current ( $I_{pa}$  = 4.6  $\mu$ A) and reduction peak current ( $I_{pc}$  = -0.8  $\mu$ A), whereas the NGSs/GCE had a significant improvement in the currents ( $I_{pa}$  = 13.9  $\mu$ A and  $I_{pc}$  = -4.8  $\mu$ A). This significant improvement in the redox peaks may have appeared because of the appreciable catalytic impact of NGSs for the DA oxidation and reduction.

### 3.3. Effect of Scan Rate

The CVs were recorded for DA (150.0  $\mu$ M) on the NGSs/GCE under variable scan rates (Figure 6). There was an apparent gradual elevation in the redox peaks achieved by raising the scan rate range from 10 to 500 mV/s. As seen in Figure 6 (inset), the anodic peak current ( $I_{pa}$ ) and cathodic peak current ( $I_{pc}$ ) had a linear association with the scan

rate square root ( $v^{1/2}$ ). This result indicates that a diffusion-controlled DA redox reaction occurs on the NGSs/GCE.

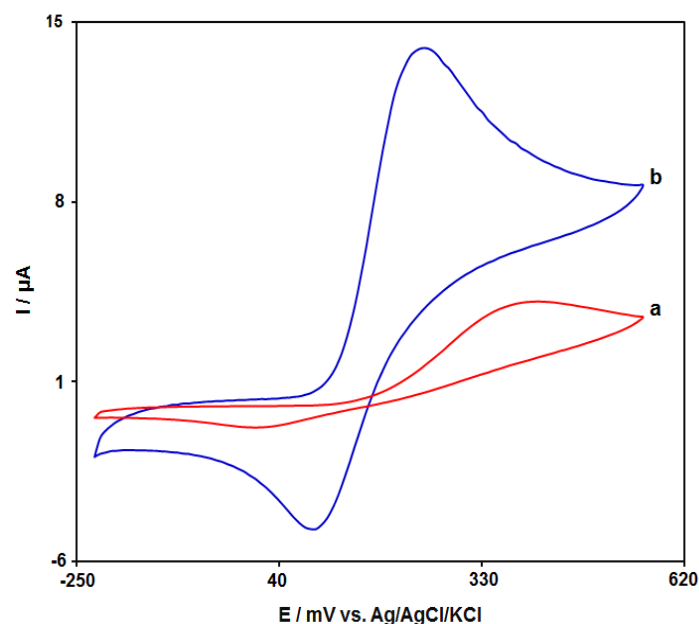


**Figure 5.** CVs captured for DA (200.0  $\mu\text{M}$ ) in PBS (0.1 M; pH = 7.0) on (a) bare GCE and (b) NGSs/GCE with a scan rate of 50 mV/s.

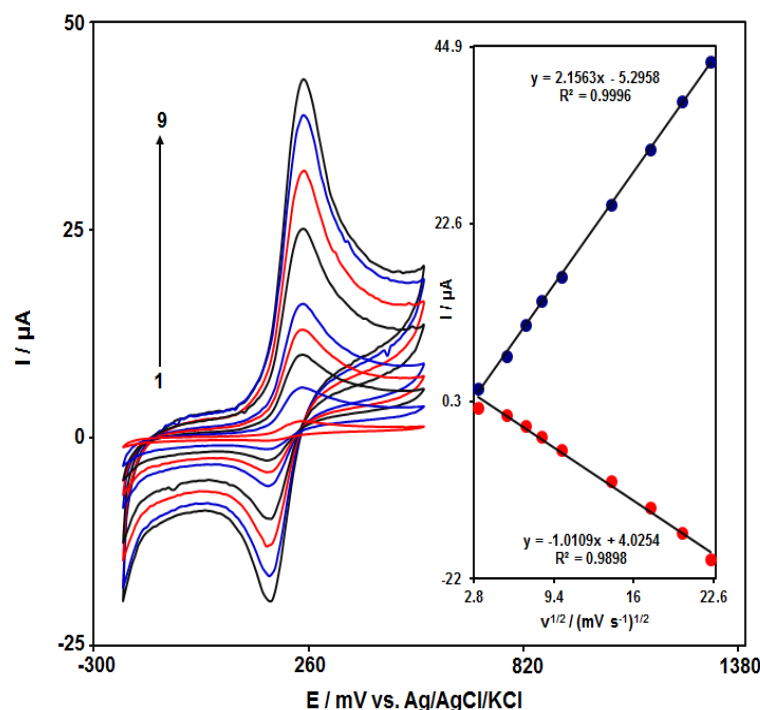


**Figure 6.** CVs captured for the DA (150.0  $\mu\text{M}$ ) on the NGSs/GCE under variable scan rates (1:10, 2:30, 3:50, 4:70, 5:100, 6:200, 7:300, 8:400, and 9:500  $\text{mV s}^{-1}$ ). Inset: the correlation of  $I_{pa}$  and  $I_{pc}$  of DA with  $v^{1/2}$ .

A Tafel plot (Figure 7 (inset)) was created on the basis of data related to the rising domain of the current–voltage curve from the linear sweep voltammogram at a low scan rate (10 mV/s) for DA (150.0  $\mu\text{M}$ ) to explore the rate-determining step. The linearity of the E vs.  $\log I$  plot clarifies the involvement of electrode-process kinetics. The slope from this

plot presents the count of transferred electrons during the rate-determining step. Based on Figure 7 (inset), the Tafel slope was estimated to be 0.091 V for the linear domain of the plot. The Tafel slope value reveals that the rate-limiting step is a one-electron transfer process considering a transfer coefficient ( $\alpha$ ) of 0.35.

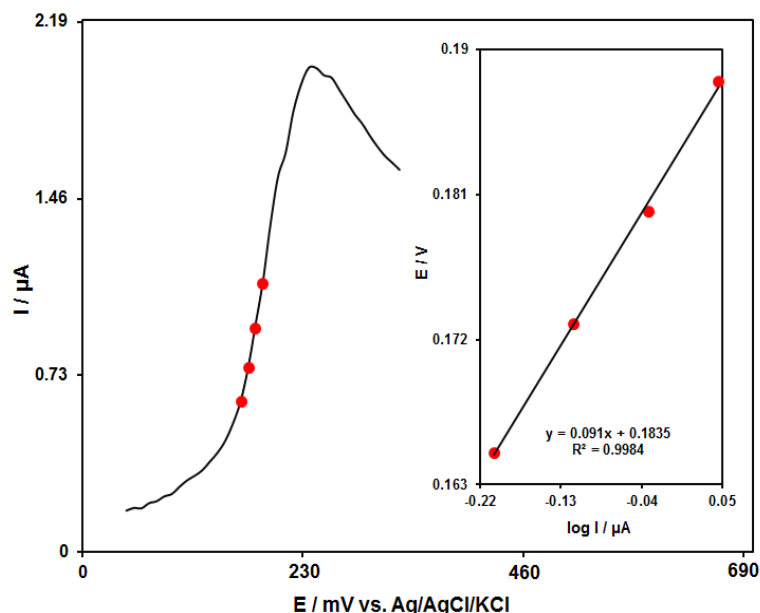


**Figure 7.** LSV for DA (150.0  $\mu\text{M}$ ) at the scan rate of 10 mV/s. Inset: the Tafel plot from the rising domain or the respective voltammogram.

### 3.4. Calibration Curve (DPV Analysis of DA)

DPV analysis was performed for variable DA contents to explore the linear dynamic range, LOD, and sensitivity of the N-GSs/GCE under optimized experimental circumstances (Figure 8). As expected, the elevation in DA level enhanced the peak current. Figure 8 (inset) shows a linear proportional of the oxidation peak currents to variable DA contents (0.1  $\mu\text{M}$  to 700.0  $\mu\text{M}$ ), with the linear regression equation of  $I_{pa} (\mu\text{A}) = 0.0625C_{DA} + 1.1884$  ( $R^2 = 0.9996$ ) and a sensitivity of 0.0625  $\mu\text{A}/\mu\text{M}$ . The LOD was estimated at 30.0 nM for DA determination on N-GSs/GCE. Table 1 compares the efficiency of the DA sensor prepared by the N-GSs-modified GCE and other reported works.

**Table 1.** Comparison of the efficiency of the NGSs/GCE sensor with other reported modified electrodes for DA determination.

Electrochemical Sensor	Electrochemical Method	Linear Range	LOD	Ref.
N-doped graphene quantum dots–chitosan nanocomposite/screen printed carbon electrode	DPV	1–100 and 100–200 $\mu\text{M}$	0.145 $\mu\text{M}$	[61]
Au-Cu <sub>2</sub> O/reduced graphene oxide/glassy carbon electrode	DPV	10–90 $\mu\text{M}$	3.9 $\mu\text{M}$	[62]
Au nanoparticle–ZnO nanocone arrays/graphene foam electrode	DPV	-	0.04 $\mu\text{M}$	[63]
Ni-based metal–organic framework/GCE		0.2–100.0 $\mu\text{M}$	60 nM	[64]
Graphene quantum dots /glassy carbon electrode	DPV	0.4–100 $\mu\text{M}$	0.05 $\mu\text{M}$	[65]
Polypyrrole–mesoporous silica molecular sieves (MCM-48)/Au electrode	Square-wave voltammetry	2–250 $\mu\text{M}$	0.7 $\mu\text{M}$	[66]
Hierarchical MnO <sub>2</sub> nanoflower/multiwalled carbon nanotube nanocomposite/glassy carbon electrode	DPV	0.5–30.0 $\mu\text{M}$	0.17 $\mu\text{M}$	[67]
NGSs/GCE	DPV	0.1–700.0 $\mu\text{M}$	30.0 nM	This work

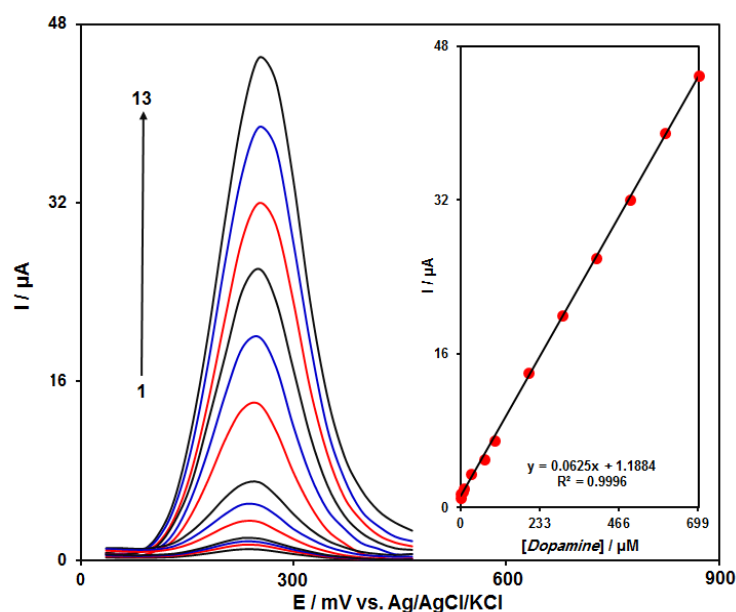


**Figure 8.** DPVs captured for the variable DA contents on the N-GSs/GCE (1–13: 0.1, 1.0, 5.0, 10.0, 30.0, 70.0, 100.0, 200.0, 300.0, 400.0, 500.0, 600.0, and 700.0  $\mu\text{M}$ ); Inset: calibration curve of voltammetric response against DA level.

### 3.5. DPV Analysis of DA in the Presence of AA and UA

Electrochemical detection of DA concurrent with AA and UA on the surface of bare electrode entails interference due to the comparatively close oxidation potentials of the three substances. Hence, the analyte concentration needed to be changed simultaneously to obtain the DPVs (Figure 9). There were three well-separated signals with the potential differences of 140 mV for AA and DA as well as 145 mV for DA and UA. Therefore, oxidation of these compounds on NGSs/GCE occurred independently, i.e., it is possible to simultaneously determine these analytes with no significant interference.

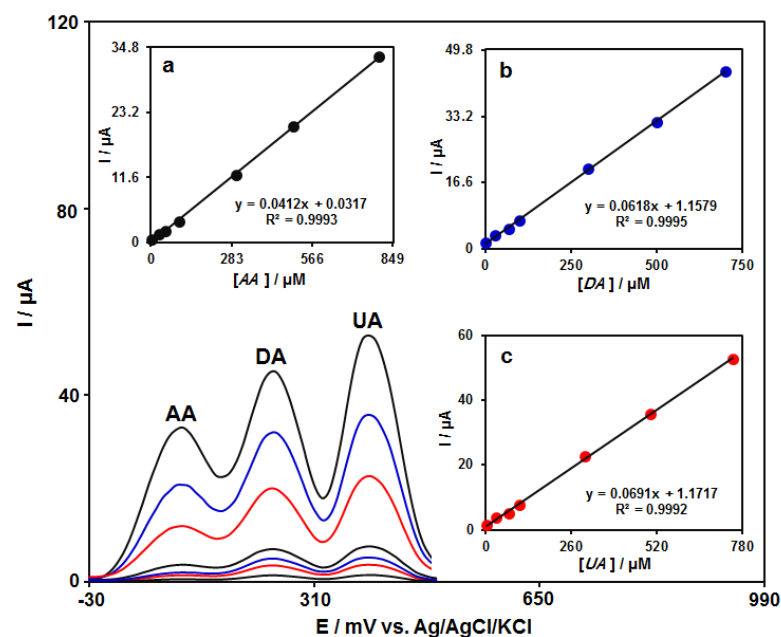


**Figure 9.** DPVs of NGSs/GCE in 0.1 M PBS (pH 7.0) with different contents of AA + DA + UA (bottom-up: 1.0 + 1.0 + 1.0, 30.0 + 30.0 + 30.0, 50.0 + 70.0 + 70.0, 100.0 + 100.0 + 100.0, 300.0 + 300.0 + 300.0, 500.0 + 500.0 + 500.0, and 800.0 + 700.0 + 750.0  $\mu\text{M}$ ). Insets: the plot of peak current versus AA concentration (a), DA concentration (b), and UA concentration (c).

### 3.6. Real Samples Analysis

The practical applicability of the N-GSs/GCE was tested by sensing AA, DA, and UA in a DA ampoule, a AA ampoule, and urine samples using the DPV procedure and standard addition method, the results of which can be seen in Table 2. The recovery rate was between 96.0% and 103.5% and all RSD values were  $\leq 3.4\%$ . According to the experimental results, the N-GSs/GCE sensor possesses high potential for practical applicability.

**Table 2.** Voltammetric sensing of AA, DA, and UA in real specimens using N-GSs/GCE. All concentrations are in  $\mu\text{A}$  ( $n = 5$ ).

Sample	Spiked ( $\mu\text{M}$ )			Found ( $\mu\text{M}$ )			Recovery (%)			(% R.S.D.)		
	AA	DA	UA	AA	DA	UA	AA	DA	UA	AA	DA	UA
DA Ampule	0	0	0	-	5.0	-	-	-	-	-	2.9	-
	5.0	2.0	6.0	4.9	7.3	6.1	98.0	104.3	101.7	3.5	1.9	2.3
	7.5	3.0	7.0	7.6	7.9	7.3	101.3	98.7	104.3	1.7	3.4	1.6
	10.0	4.0	8.0	9.9	9.1	7.7	99.0	101.1	96.2	2.9	2.2	3.0
	12.5	5.0	9.0	12.8	9.6	8.9	102.4	96.0	98.9	2.8	2.4	2.3
AA Ampule	0	0	0	3.5	-	-	-	-	-	3.4	-	-
	2.0	4.5	4.0	5.6	4.4	4.1	101.8	97.8	102.5	2.0	1.9	3.4
	4.0	6.5	5.0	7.3	6.7	4.8	97.3	103.1	96.0	2.9	3.5	1.8
	6.0	8.5	6.0	9.4	8.4	6.1	98.9	98.8	101.7	2.4	2.7	2.5
	8.0	10.5	7.0	11.9	10.6	6.8	103.5	100.9	97.1	2.6	2.1	2.9
Urine	0	0	0	-	-	3.0	-	-	-	-	-	3.1
	5.0	6.0	3.0	4.9	6.2	5.9	98.0	103.3	98.3	3.4	2.3	1.7
	10.0	8.0	4.0	10.3	7.8	7.1	103.0	97.5	101.4	2.4	2.6	3.0
	15.0	10.0	5.0	14.9	10.1	7.7	99.3	101.0	96.2	1.6	3.1	2.1
	20.0	12.0	6.0	20.2	11.9	9.3	101.0	99.2	103.3	2.9	1.9	2.3

## 4. Conclusions

The present research developed a new sensor (N-GSs/GCE) for determination of DA. The analytical findings highlighted commendable electrocatalytic performance of the proposed sensor (N-GSs/GCE) for DA detection. The peak current of DA oxidation had a linear relationship with variable concentrations (0.1–700.0  $\mu\text{M}$ ), with a thin LOD (30.0 nM). The modified electrode could successfully determine the DA in the presence of UA and AA. The practical applicability of the as-developed N-GSs/GCE sensor was verified by sensing the study analytes in real specimens, with satisfactory recovery rates. These results suggest the proposed electrode has excellent performance and may be used for future DA detection probes based on electrochemical techniques.

**Author Contributions:** Conceptualization, H.M. and H.B.; methodology, H.M. and H.B.; validation, H.M. and H.B.; formal analysis, H.M.; investigation, H.B.; writing—original draft preparation H.M. and H.B.; writing—review and editing, H.M. and H.B.; supervision, H.B.; project administration, H.B. All authors have read and agreed to the published version of the manuscript.

**Funding:** This research was funded by Graduate University of Advanced Technology, Kerman, Iran.

**Data Availability Statement:** The data presented in this study are available upon request from the corresponding authors.

**Conflicts of Interest:** The authors declare no conflict of interest.

## References

1. O'Neill, R.D. Microvoltammetric techniques and sensors for monitoring neurochemical dynamics in vivo. *Analyst* **1994**, *119*, 767–779. [[CrossRef](#)]
2. Fayemi, O.E.; Adekunle, A.S.; Swamy, B.K.; Ebenso, E.E. Electrochemical sensor for the detection of dopamine in real samples using polyaniline/NiO, ZnO, and Fe<sub>3</sub>O<sub>4</sub> nanocomposites on glassy carbon electrode. *J. Electroanal. Chem.* **2018**, *818*, 236–249. [[CrossRef](#)]
3. Jin, H.; Zhao, C.; Gui, R.; Gao, X.; Wang, Z. Reduced graphene oxide/nile blue/gold nanoparticles complex-modified glassy carbon electrode used as a sensitive and label-free aptasensor for ratiometric electrochemical sensing of dopamine. *Anal. Chim. Acta* **2018**, *1025*, 154–162. [[CrossRef](#)]
4. Morón, J.A.; Brockington, A.; Wise, R.A.; Rocha, B.A.; Hope, B.T. Dopamine uptake through the norepinephrine transporter in brain regions with low levels of the dopamine transporter: Evidence from knock-out mouse lines. *J. Neurosci.* **2002**, *15*, 389–395. [[CrossRef](#)]
5. Yamamoto, B.K.; Novotney, S. Regulation of extracellular dopamine by the norepinephrine transporter. *J. Neurochem.* **1998**, *71*, 274–280. [[CrossRef](#)]
6. Zhang, L.; Hou, Y.; Lv, C.; Liu, W.; Zhang, Z.; Peng, X. Copper-based metal–organic xerogels on paper for chemiluminescence detection of dopamine. *Anal. Methods* **2020**, *12*, 4191–4198. [[CrossRef](#)]
7. Lin, Z.; Wang, H.; Hu, L.; Li, J.; Lin, J.; Liu, B.; Zhao, Z.; Rao, Y. Simultaneous determination of N-ethylpentylone, dopamine, 5-hydroxytryptamine and their metabolites in rat brain microdialysis by liquid chromatography tandem mass spectrometry. *Biomed. Chromatogr.* **2019**, *33*, e4626. [[CrossRef](#)]
8. Wang, J.; Hu, Y.; Zhou, Q.; Hu, L.; Fu, W.; Wang, Y. Peroxidase-like activity of metal–organic framework [Cu (PDA)(DMF)] and its application for colorimetric detection of dopamine. *ACS Appl. Mater. Interfaces* **2019**, *11*, 44466–44473. [[CrossRef](#)] [[PubMed](#)]
9. Ma, Y.; Chen, A.Y.; Xie, X.F.; Wang, X.Y.; Wang, D.; Wang, P.; Li, H.J.; Yang, J.H.; Li, Y. Doping effect and fluorescence quenching mechanism of N-doped graphene quantum dots in the detection of dopamine. *Talanta* **2019**, *196*, 563–571. [[CrossRef](#)] [[PubMed](#)]
10. Roychoudhury, A.; Francis, K.A.; Patel, J.; Jha, S.K.; Basu, S. A decoupler-free simple paper microchip capillary electrophoresis device for simultaneous detection of dopamine, epinephrine and serotonin. *RSC Adv.* **2020**, *10*, 25487–25495. [[CrossRef](#)]
11. Karimi-Maleh, H.; Sheikhsheoie, M.; Sheikhsheoie, I.; Ranjbar, M.; Alizadeh, J.; Maxakato, N.W.; Abbaspourrad, A. A novel electrochemical epinine sensor using amplified CuO nanoparticles and an-hexyl-3-methylimidazolium hexafluorophosphate electrode. *New J. Chem.* **2019**, *43*, 2362–2367. [[CrossRef](#)]
12. Shivanna, M.; Manjunath, S.; Sidlingappa, M.; Dharmaparakash, M.S. Electrochemical Detection of Serotonin Using t-ZrO<sub>2</sub> Nanoparticles Modified Carbon Paste Electrode. *J. Electrochem. Soc.* **2020**, *167*, 155512.
13. Kouadio, K.E.; Kambiré, O.; Koffi, K.S.; Ouattara, L. Electrochemical oxidation of paracetamol on boron-doped diamond electrode: Analytical performance and paracetamol degradation. *J. Electrochem. Sci. Eng.* **2021**, *11*, 71–86.
14. Payehghadr, M.; Taherkhani, Y.; Maleki, A.; Nourifard, F. Selective and sensitive voltammetric sensor for methocarbamol determination by molecularly imprinted polymer modified carbon paste electrode. *Eurasian Chem. Commun.* **2020**, *2*, 982–990.
15. Deshmukh, M.A.; Celiesiute, R.; Ramanaviciene, A.; Shirsat, M.D.; Ramanavicius, A. EDTA\_PANI/SWCNTs nanocomposite modified electrode for electrochemical determination of copper (II), lead (II) and mercury (II) ions. *Electrochim. Acta* **2018**, *259*, 930–938. [[CrossRef](#)]
16. Raof, J.B.; Ojani, R.; Beitollahi, H. Electrocatalytic determination of ascorbic acid at chemically modified carbon paste electrode with 2,7-bis (ferrocenyl ethynyl) fluoren-9-one. *Int. J. Electrochem. Sci.* **2007**, *2*, 534–548.
17. Rshad, S.; Mofidi-Rasi, R. Electrocatalytic oxidation of sulfite Ion at the surface carbon ceramic modified electrode with prussian blue. *Eurasian Chem. Commun.* **2019**, *1*, 43–52.
18. Kumar, D.R.; Baynosa, M.L.; Dhakal, G.; Shim, J.J. Sphere-like Ni<sub>3</sub>S<sub>4</sub>/NiS<sub>2</sub>/MoOx composite modified glassy carbon electrode for the electrocatalytic determination of d-penicillamine. *J. Mol. Liq.* **2020**, *301*, 112447. [[CrossRef](#)]
19. Mohanraj, J.; Durgalakshmi, D.; Rakkesh, R.A.; Balakumar, S.; Rajendran, S.; Karimi-Maleh, H. Facile synthesis of paper based graphene electrodes for point of care devices: A double stranded DNA (dsDNA) biosensor. *J. Colloid Interface Sci.* **2020**, *566*, 463–472. [[CrossRef](#)]
20. Karimi-Maleh, H.; Karimi, F.; Orooji, Y.; Mansouri, G.; Razmjou, A.; Aygun, A.; Sen, F. A new nickel-based co-crystal complex electrocatalyst amplified by NiO dope Pt nanostructure hybrid; a highly sensitive approach for determination of cysteamine in the presence of serotonin. *Sci. Rep.* **2020**, *10*, 11699. [[CrossRef](#)]
21. Montazarolmahdi, M.; Masrounia, M.; Nezhadali, A. A new electrochemical approach for the determination of phenylhydrazine in water and wastewater samples using amplified carbon paste electrode. *Chem. Methodol.* **2020**, *4*, 732–742.
22. Wang, L.; Yang, R.; Qu, L.; Harrington, P.D.B. Electrostatic repulsion strategy for high-sensitive and selective determination of dopamine in the presence of uric acid and ascorbic acid. *Talanta* **2020**, *210*, 120626. [[CrossRef](#)]
23. Shashikumara, J.K.; Swamy, B.K. Electrochemical investigation of dopamine in presence of uric acid and ascorbic acid at poly (reactive blue) modified carbon paste electrode: A voltammetric study. *Sens. Int.* **2020**, *1*, 100008. [[CrossRef](#)]
24. Kunpatee, K.; Traipop, S.; Chailapakul, O.; Chuanuwatanakul, S. Simultaneous determination of ascorbic acid, dopamine, and uric acid using graphene quantum dots/ionic liquid modified screen-printed carbon electrode. *Sens. Actuators B Chem.* **2020**, *314*, 128059. [[CrossRef](#)]

25. Mahalakshmi, S.; Sridevi, V. In situ electrodeposited gold nanoparticles on polyaniline-modified electrode surface for the detection of dopamine in presence of ascorbic acid and uric acid. *Electrocatalysis* **2021**, *12*, 415–435. [[CrossRef](#)]
26. Beitollahi, H.; Khalilzadeh, M.A.; Tajik, S.; Safaei, M.; Zhang, K.; Jang, H.W.; Shokouhimehr, M. Recent advances in applications of voltammetric sensors modified with ferrocene and its derivatives. *ACS Omega* **2020**, *5*, 2049–2059. [[CrossRef](#)] [[PubMed](#)]
27. Pyma, H.; Roshanfekr, H.; Ansari, S. DNA-based electrochemical biosensor using chitosan–carbon nanotubes composite film for biodetection of Pirazon. *Eurasian Chem. Commun.* **2020**, *2*, 213–225.
28. Garkani-Nejad, F.; Sheikhshoae, I.; Beitollahi, H. Simultaneous detection of carmoisine and tartrazine in food samples using GO-Fe<sub>3</sub>O<sub>4</sub>-PAMAM and ionic liquid based electrochemical sensor. *Food Chem. Toxicol.* **2022**, *162*, 112864. [[CrossRef](#)]
29. Abrishamkar, M.; Ehsani-Tilami, S.; Hosseini-Kaldozakh, S. Electrocatalytic oxidation of cefixime at the surface of modified carbon paste electrode with synthesized nano zeolite. *Adv. J. Chem. A* **2020**, *3*, 767–776.
30. Kamble, B.; Garadkar, K.M.; Sharma, K.K.; Kamble, P.; Tayade, S.; Ajalkar, B.D. Determination of 4-nitrophenol using MoO<sub>3</sub> loaded glassy carbon electrode via electrochemical sensing approach. *J. Electrochem. Sci. Eng.* **2021**, *11*, 143–159. [[CrossRef](#)]
31. Tajik, S.; Beitollahi, H.; Torkzadeh-Mahani, M. Electrochemical immunosensor for the detection of anti-thyroid peroxidase antibody by gold nanoparticles and ionic liquid-modified carbon paste electrode. *J. Nanostruct. Chem.* **2022**, *12*, 581–588. [[CrossRef](#)]
32. Shetti, N.P.; Nayak, D.S.; Malode, S.J.; Kulkarni, R.M. An electrochemical sensor for clozapine at ruthenium doped TiO<sub>2</sub> nanoparticles modified electrode. *Sens. Actuators B Chem.* **2017**, *247*, 858–867. [[CrossRef](#)]
33. Karimi-Maleh, H.; Darabi, R.; Shabani-Nooshabadi, M.; Baghayeri, M.; Karimi, F.; Rouhi, J.; Karaman, C. Determination of D&C Red 33 and Patent Blue V Azo dyes using an impressive electrochemical sensor based on carbon paste electrode modified with ZIF-8/g-C<sub>3</sub>N<sub>4</sub>/Co and ionic liquid in mouthwash and toothpaste as real samples. *Food Chem. Toxicol.* **2022**, *162*, 112907.
34. Mirbaloochzehi, M.R.; Rezvani, A.; Samimi, A.; Shayesteh, M. Application of a novel surfactant-modified natural nano-zeolite for removal of heavy metals from drinking water. *Adv. J. Chem. A* **2020**, *3*, 612–620.
35. Zhang, L.; Guo, H.; Xue, R.; Yue, L.; Li, Q.; Liu, H.; Yang, W. In-situ facile synthesis of flower shaped NiS<sub>2</sub>@regenerative graphene oxide derived from waste dry battery nano-composites for high-performance supercapacitors. *J. Energy Storage* **2020**, *31*, 101630. [[CrossRef](#)]
36. Beitollahi, H.; Garkani Nejad, F.; Dourandish, Z.; Tajik, S. A novel voltammetric amaranth sensor based on screen printed electrode modified with polypyrrole nanotubes. *Environ. Res.* **2022**, *214*, 113725. [[CrossRef](#)]
37. Mohammadi, S.S.; Ghasemi, N.; Ramezani, M. Bio-fabrication of silver nanoparticles using naturally available wild herbaceous plant and its antibacterial activity. *Eurasian Chem. Commun.* **2020**, *2*, 87–102.
38. Karimi-Maleh, H.; Karaman, C.; Karaman, O.; Karimi, F.; Vasseghian, Y.; Fu, L.; Mirabi, A. Nanochemistry approach for the fabrication of Fe and N co-decorated biomass-derived activated carbon frameworks: A promising oxygen reduction reaction electrocatalyst in neutral media. *J. Nanostruct. Chem.* **2022**, *12*, 429–439. [[CrossRef](#)]
39. Kashkooli, F.M.; Soltani, M.; Souri, M. Controlled anti-cancer drug release through advanced nano-drug delivery systems: Static and dynamic targeting strategies. *J. Control. Release* **2020**, *327*, 316–349. [[CrossRef](#)]
40. Khakyzadeh, V.; Rezaei-Vahidian, H.; Sediqi, S.; Azimi, S.; Karimi-Nami, R. Programming adsorptive removal of organic azo dye from aqueous media using magnetic carbon nano-composite. *Chem. Methodol.* **2021**, *5*, 324–330.
41. Karimi-Maleh, H.; Cellat, K.; Arıkan, K.; Savk, A.; Karimi, F.; Şen, F. Palladium–nickel nanoparticles decorated on functionalized-MWCNT for high precision non-enzymatic glucose sensing. *Mater. Chem. Phys.* **2020**, *250*, 123042. [[CrossRef](#)]
42. Shi, R.; Liang, J.; Zhao, Z.; Liu, A.; Tian, Y. An electrochemical bisphenol A sensor based on one step electrochemical reduction of cuprous oxide wrapped graphene oxide nanoparticles modified electrode. *Talanta* **2017**, *169*, 37–43. [[CrossRef](#)] [[PubMed](#)]
43. Miraki, M.; Karimi-Maleh, H.; Taher, M.A.; Cheraghi, S.; Karimi, F.; Agarwal, S.; Gupta, V.K. Voltammetric amplified platform based on ionic liquid/NiO nanocomposite for determination of benserazide and levodopa. *J. Mol. Liq.* **2019**, *278*, 672–676. [[CrossRef](#)]
44. Sadeghi, H.; Shahidi, S.A.; Naghizadeh Raeisi, S.; Ghorbani-HasanSaraei, A.; Karimi, F. Electrochemical determination of folic acid in fruit juices samples using electroanalytical sensor amplified with CuO/SWCNTs and 1-butyl-2,3-dimethylimidazolium hexafluorophosphate. *Chem. Methodol.* **2020**, *4*, 743–753.
45. Baghizadeh, A.; Karimi-Maleh, H.; Khoshnama, Z.; Hassankhani, A.; Abbasghorbani, M. A voltammetric sensor for simultaneous determination of vitamin C and vitamin B<sub>6</sub> in food samples using ZrO<sub>2</sub> nanoparticle/ionic liquids carbon paste electrode. *Food Anal. Methods* **2015**, *8*, 549–557. [[CrossRef](#)]
46. Emir, G.; Dilgin, Y.; Ramanaviciene, A.; Ramanavicius, A. Amperometric nonenzymatic glucose biosensor based on graphite rod electrode modified by Ni-nanoparticle/polypyrrole composite. *Microchem. J.* **2021**, *161*, 105751. [[CrossRef](#)]
47. Garkani-Nejad, F.; Beitollahi, H.; Alizadeh, R. Sensitive determination of hydroxylamine on ZnO nanorods/graphene oxide nanosheets modified graphite screen printed electrode. *Anal. Bioanal. Electrochem.* **2017**, *9*, 134–144.
48. Sengar, M.; Saxena, S.; Satsangee, S.; Jain, R. Silver nanoparticles decorated functionalized multiwalled carbon nanotubes modified screen printed sensor for the voltammetric determination of butorphanol. *J. Appl. Organomet. Chem.* **2021**, *1*, 95–108.
49. Beitollahi, H.; Tajik, S.; Aflatoonian, M.R.; Makarem, A. Glutathione detection at carbon paste electrode modified with ethyl 2-(4-ferrocenyl-[1,2,3]triazol-1-yl)acetate, ZnFe<sub>2</sub>O<sub>4</sub> nanoparticles and ionic liquid. *J. Electrochem. Sci. Eng.* **2022**, *12*, 209–217. [[CrossRef](#)]

50. Sunder, G.S.S.; Rohanifar, A.; Devasurendra, A.M.; Kirchoff, J.R. Selective determination of l-DOPA at a graphene oxide/yttrium oxide modified glassy carbon electrode. *Electrochim. Acta* **2019**, *301*, 192–199. [[CrossRef](#)]
51. Ren, Q.; Shen, X.; Sun, Y.; Fan, R.; Zhang, J. A highly sensitive competitive immunosensor based on branched polyethyleneimine functionalized reduced graphene oxide and gold nanoparticles modified electrode for detection of melamine. *Food Chem.* **2020**, *304*, 125397. [[CrossRef](#)] [[PubMed](#)]
52. Karimi-Maleh, H.; Arotiba, O.A. Simultaneous determination of cholesterol, ascorbic acid and uric acid as three essential biological compounds at a carbon paste electrode modified with copper oxide decorated reduced graphene oxide nanocomposite and ionic liquid. *J. Colloid Interface Sci.* **2020**, *560*, 208–212. [[CrossRef](#)]
53. Barsan, M.M.; Prathish, K.P.; Sun, X.; Brett, C.M. Nitrogen doped graphene and its derivatives as sensors and efficient direct electron transfer platform for enzyme biosensors. *Sens. Actuators B Chem.* **2014**, *203*, 579–587. [[CrossRef](#)]
54. Xing, H.; Xu, J.; Zhu, X.; Duan, X.; Lu, L.; Wang, W.; Shang, Y.; Yang, T. Highly sensitive simultaneous determination of cadmium (II), lead (II), copper (II), and mercury (II) ions on N-doped graphene modified electrode. *J. Electroanal. Chem.* **2016**, *760*, 52–58. [[CrossRef](#)]
55. Fan, H.; Li, Y.; Wu, D.; Ma, H.; Mao, K.; Fan, D.; Du, B.; Li, H.; Wei, Q. Electrochemical bisphenol A sensor based on N-doped graphene sheets. *Anal. Chim. Acta* **2012**, *711*, 24–28. [[CrossRef](#)]
56. Yan, Y.; Jamal, R.; Yu, Z.; Zhang, R.; Zhang, W.; Ge, Y.; Liu, Y.; Abdiryim, T. Composites of thiol-grafted PEDOT with N-doped graphene or graphitic carbon nitride as an electrochemical sensor for the detection of paracetamol. *J. Mater. Sci.* **2020**, *55*, 5571–5586.
57. Bai, L.; Chen, Y.; Liu, X.; Zhou, J.; Cao, J.; Hou, L.; Guo, S. Ultrasensitive electrochemical detection of Mycobacterium tuberculosis IS6110 fragment using gold nanoparticles decorated fullerene nanoparticles/nitrogen-doped graphene nanosheet as signal tags. *Anal. Chim. Acta* **2019**, *1080*, 75–83. [[CrossRef](#)] [[PubMed](#)]
58. Bard, A.J.; Faulkner, L.R. *Electrochemical Methods: Fundamentals and Applications*, 2nd ed.; John Wiley & Sons: New York, NY, USA, 2001.
59. Liu, Y.; Ma, J.; Wu, T.; Wang, X.; Huang, G.; Liu, Y.; Qiu, H.; Li, Y.; Wang, W.; Gao, J. Cost-effective reduced graphene oxide-coated polyurethane sponge as a highly efficient and reusable oil-absorbent. *ACS Appl. Mater. Interfaces* **2013**, *5*, 10018–10026. [[CrossRef](#)]
60. Rahmani, Z.; Rashidi, A.M.; Samadi, M.T.; Rahmani, A.R. N-doped reduced graphene oxide aerogel for the selective adsorption of oil pollutants from water: Isotherm and kinetic study. *J. Ind. Eng. Chem.* **2018**, *61*, 416–426. [[CrossRef](#)]
61. Ben Aoun, S. Nanostructured carbon electrode modified with N-doped graphene quantum dots–chitosan nanocomposite: A sensitive electrochemical dopamine sensor. *R. Soc. Open Sci.* **2017**, *4*, 171199. [[CrossRef](#)] [[PubMed](#)]
62. Aparna, T.K.; Sivasubramanian, R.; Dar, M.A. One-pot synthesis of Au-Cu<sub>2</sub>O/rGO nanocomposite based electrochemical sensor for selective and simultaneous detection of dopamine and uric acid. *J. Alloys Compd.* **2018**, *741*, 1130–1141. [[CrossRef](#)]
63. Yue, H.Y.; Zhang, H.J.; Huang, S.; Lu, X.X.; Gao, X.; Song, S.S.; Wang, Z.; Wang, W.Q.; Guan, E.H. Highly sensitive and selective dopamine biosensor using Au nanoparticles-ZnO nanocone arrays/graphene foam electrode. *Mater. Sci. Eng. C* **2020**, *108*, 110490. [[CrossRef](#)]
64. Huang, Z.; Zhang, L.; Cao, P.; Wang, N.; Lin, M. Electrochemical sensing of dopamine using a Ni-based metal-organic framework modified electrode. *Ionics* **2021**, *27*, 1339–1345. [[CrossRef](#)]
65. Zheng, S.; Huang, R.; Ma, X.; Tang, J.; Li, Z.; Wang, X.; Wei, J.; Wang, J. A highly sensitive dopamine sensor based on graphene quantum dots modified glassy carbon electrode. *Int. J. Electrochem. Sci.* **2018**, *13*, 5723. [[CrossRef](#)]
66. Zablocka, I.; Wysocka-Zolopa, M.; Winkler, K. Electrochemical detection of dopamine at a gold electrode modified with a polypyrrole-mesoporous silica molecular sieves (MCM-48) film. *Int. J. Mol. Sci.* **2019**, *20*, 111. [[CrossRef](#)] [[PubMed](#)]
67. Wang, Y.; Wang, L.; Zhuang, Q. A ratiometric electrochemical sensor for dopamine detection based on hierarchical manganese dioxide nanoflower/multiwalled carbon nanotube nanocomposite modified glassy carbon electrode. *J. Alloys Compd.* **2019**, *802*, 326–334. [[CrossRef](#)]